Circuit-Parameter-Independent Nonlinearity Compensation for Boost Converter Operated in Discontinuous Current Mode

Hoai Nam Le, *Student Member, IEEE*, Koji Orikawa, *Member, IEEE*
and Jun-Ichi Itoh, *Senior Member, IEEE*

***Abstract*—This paper proposes a current control method for discontinuous current mode (DCM) in order to achieve the same control performance as continuous current mode (CCM) in a boost converter. By utilizing the duty ratio at the previous calculation period to compensate for a DCM nonlinearity, the controller which is designed for CCM can also be used in DCM. In the frequency analysis, the cutoff frequency of the proposed DCM current control agrees exactly to the design value which is 2 kHz, whereas the cutoff frequency of the conventional DCM current control results in high error of 47.5%. In the current step response experiment with a 360-W prototype and the switching frequency of 20 kHz, the experimental DCM current response almost agrees with the conventional CCM current response, which are 380-μs rise time for both CCM and DCM, 9% and 8% overshoot for CCM and DCM, respectively. Furthermore, the computation time of the proposed DCM current control is shorter 35% than the conventional DCM current control.**

***Index Terms*—Current control, DC-DC power converters, Discontinuous current mode, Nonlinear control systems.**

I. Introduction

TYPICAL boost DC-DC converters are widely applied in many power conversion systems, e.g. power conditioning system in photo-voltaic systems. The problem in the typical boost converters is the use of bulky passive components, i.e. an output capacitor and a boost inductor. One of the challenges to minimize the output capacitor is the dynamic voltage regulation during the fast load transient. In the applications for power conditioning system, the output voltage within a tight tolerance range must be maintained during the faults of the grid, i.e. a load current step occurs. The load transient requirement can be met even with small capacitance by a wide bandwidth voltage control [1]-[2]. On the other hand, many minimization methods for the inductor have been proposed such as high frequency switching, coupled-inductor or flying-capacitor topologies [3]-[6]. However, higher switching frequency leads to the increase in both the switching loss and the emission noise [7], whereas the addition components results in the complexity of the design in the main circuit and the control method.

There are other approaches to minimize the boost inductor in terms of the operation mode. By increasing the current ripple at a given switching frequency, the typical boost converters can be operated in two main current modes; continuous current mode (CCM) and discontinuous current mode (DCM) [8]-[9]. The advantages of CCM are: simple controller design due to the linear duty-ratio-to-inductor-current transfer function, and the simple average current sampling. On the other hand, the boost converter with the DCM operation achieves the high efficiency over a wide load range because the current ripple in DCM decreases at light load. Nonetheless, the nonlinear duty-ratio-to-current transfer occurs in DCM, which worsens the current control performance when the same controller as in CCM is used. In particular, the effects of the DCM nonlinearity on the duty-ratio-to-current transfer function changes according to the current load [10]. This results in the overcurrent when the current is regulated by a wide bandwidth controller [11]. In past few years, many researches focusing on the control of DCM have been reported to solve this problem [12]-[17]. However, in those control methods, the DCM nonlinearity compensation method becomes circuit-parameter-dependent. Due to this problem, a wide bandwidth current control is still difficult to be applied into DCM. Consequently, the bandwidth of the voltage control cannot be increased in order to minimize the output capacitor [18], which restricts the circuit minimization.

This paper proposes a DCM nonlinearity compensation method which is independent from the boost inductance and the load condition. The original idea in this paper is that the DCM nonlinearity compensation is constructed by utilizing the duty ratio at the previous calculation period instead of using the circuit parameter. The advantages of the proposed method are as follows: circuit-parameter-independence and short computation time. This paper is organized as follows; in section II, the problems of the conventional DCM control are introduced in detail with past works, then in section III the design of the conventional PI controller is explained because the proposed DCM control is based on the CCM control with a PI controller, next the DCM nonlinearity

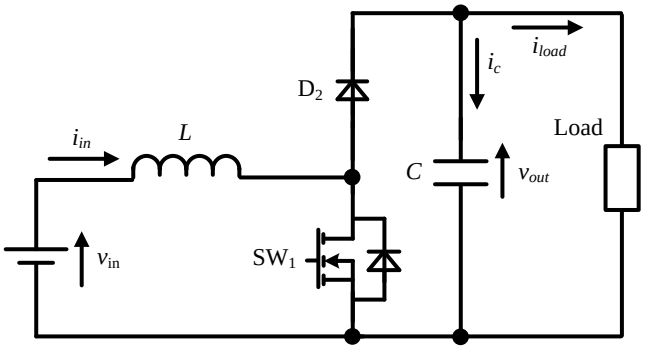

Fig. 1. Circuit diagram of typical boost converter. This paper proposed the concept where the boost inductor is minimized by DCM and the output capacitor is minimized by the wide bandwidth voltage control in DCM.

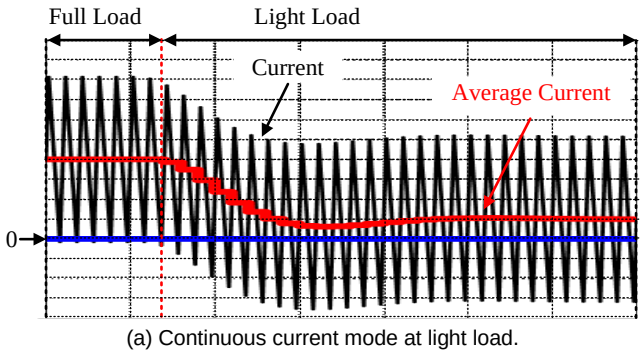

(a) Continuous current mode at light load.

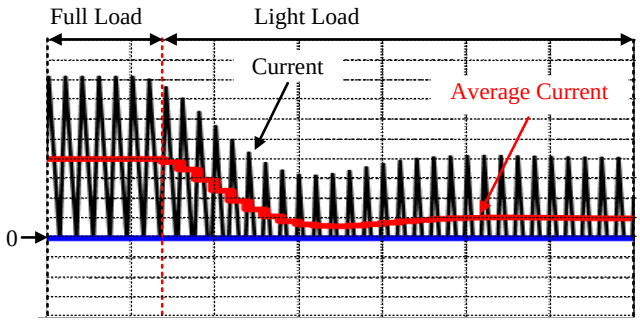

(b) Discontinuous current mode at light load.

Fig. 2. Inductor current waveform of CCM and DCM when the inductance is minimized at given switching frequency. At light load, the constant current ripple of CCM increases the ratio between the average current and the current ripple, whereas the current ripple of DCM decreases. Therefore, the high efficiency at wide load range with DCM is achievable.

compensation method is proposed as the main part of this paper. After that, the validity of the proposed DCM nonlinearity compensation method is verified in section IV. In addition, in order to achieve higher efficiency in the boost converter, the simple DCM synchronous switching method is realized based on the proposed DCM current control. Finally, the comparisons of the efficiencies and the current-control computation time are demonstrated in order to confirm the effectiveness of the proposed DCM current control.

II. Problems of Conventional Discontinuous-Current-Mode Control Methods

Fig. 1 shows the typical boost converter configuration. In order to minimize the boost converter at the given switching frequency, this paper proposed the concept where the boost inductor is minimized by the DCM operation and the output capacitor is minimized by the wide bandwidth voltage control in DCM. In other words, at the given switching frequency, the boost converter can achieve higher power density by the application of DCM. Note that the high current ripple in DCM can be overcome simply with the interleaved boost converter topologies as shown in [8]-[9].

Fig. 2 illustrates the current waveforms of CCM and DCM when the inductance is reduced at the given switching frequency. Note that the boost converter is designed to be operated at critical current mode (CRM) at full load and the constant switching frequency is applied over all load range, i.e. the requirement to apply the pulse-width modulation. At light load, the boost inductor current becomes discontinuous. Consequently, the transfer function becomes nonlinear and this leads to the instability of the current control [10]. In order to avoid the discontinuous current, the switch is used instead of the upper diode. The CCM synchronous switching by applying this switch improves the efficiency at full load and maintains the continuity of the current. However, the current ripple becomes much higher than the average current at light load. This results in the poor power conversion efficiency at light load. On the other hand, the current ripple in DCM decreases at light load as shown in Fig. 2(b). Hence, when the converter is operated in DCM, the high efficiency is expected to be maintained over wide load range.

The current control for DCM is generally divided into two main methods: feedforward control and feedback control. The principle of the DCM current feedforward control is to design the controller based on the reduced-order model or the full-order model [9], [12]. An advantage of the feedforward control is the unrequired current sensor. However, the mismatch between the nominal values and the actual values of the circuit parameters results in the instability of the control system when a wide bandwidth control is applied [11], [18]. On the other hand, the feedback control in DCM has to deal with the nonlinear duty-to-current transfer function [10]. In [13] and [17], the PI controller with constant coefficients is used in order to control DCM. The DCM nonlinearity, however, implies that the duty-ratio-to-inductor-current transfer function depends on the load. With a constant-coefficient PI controller, the cutoff frequency of current controller varies dependently on load, which results in the instability of the control system when the load varies. In order to deal with the DCM nonlinearity and also avoid the PI controller design with online-tuning coefficients, the hybrid control between the feedforward control and feedback control has been proposed in [15]-[16]. The principle of these control methods is to estimate the duty ratio from the current command, then feed forward this estimated duty ratio to compensate for the DCM nonlinearity. In [15], the estimated duty ratio is calculated by a complex function based on the reduced-order model as same as [9], [12]. In [16], the calculation time is reduced by estimating the duty ratio through a reference table.

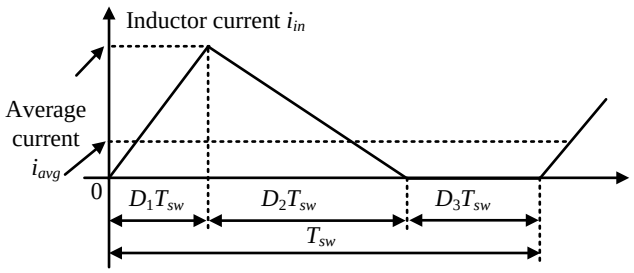

Fig. 3. Inductor current waveform in DCM. The zero current interval occurring in DCM introduces the nonlinearity into the duty-to-current transfer function [10].

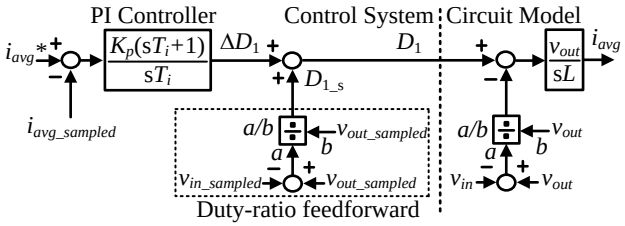

Fig. 4. Current control system for CCM. By applying the duty-ratio feedforward in CCM, the PI controller compensates only the small difference between the duty ratio at steady state and the instantaneous duty ratio [15].

However, the penalties of these control methods are as follows; the control system becomes circuit-parameter-dependent and a long computation time is required. In case of the power conditioning system application, the boost converter is usually required to deal with the severe change of the ambient environment, where the circuit condition such as the operation temperature varies frequently. When the actual values of the circuit parameters such as, e.g. inductance and capacitance, are different from the nominal values due to the variation of the circuit condition, the stability of the circuit-parameter-dependent control system can no longer be guaranteed. As the motivation for the achievement of the wide bandwidth DCM current control, it is necessary to realize the DCM nonlinearity compensation with the features as circuit-parameter-independence and short computation time.

III. Discontinuous-Current-Mode Nonlinearity Compensation by Duty Ratio at Previous Calculation Period

A. Conventional Current Loop Design in Continuous Current Mode

Fig. 3 depicts the inductor current waveform in DCM, where D_1, D_2 and D_3 denote the duty ratios of the first, the second and the zero-current interval. Average small signal modeling technique is used to model the boost converter for the inner current control loop design [10], [16]. The average inductor voltage during a switching period T_{sw} is given by (1),

$$L\frac{di_{avg}}{dt} = D_1 v_{in} + D_2\left(v_{in} - v_{out}\right) \quad \text{.....(1)}$$

where v_{in} and v_{out} are the instantaneous input voltage and the instantaneous output voltage, i_{avg} is the average inductor current during a switching period T_{sw}, and L is the inductance. In case of CCM, the relationship between D_1 and D_2 becomes,

$$D_1 + D_2 = 1 \quad \text{.....(2)}$$

By substituting (2) into (1) in order to represent (1) as a function of only the duty ratio D_1, (3) is obtained,

$$\frac{L}{v_{out}}\frac{di_{avg}}{dt} = \frac{v_{in} - v_{out}}{v_{out}} + D_1 \quad \text{.....(3)}$$

When the boost converter operates in steady state, the output voltage, the input voltage, the average input current and the duty ratio in each switching period T_{sw} can be expressed as,

$$v_{out} = V_{out\_s} + \Delta v_{out} \quad \text{.....(4)}$$

$$v_{in} = V_{in\_s} + \Delta v_{in} \quad \text{.....(5)}$$

$$i_{avg} = I_{avg\_s} + \Delta i_{avg} \quad \text{.....(6)}$$

$$D_1 = D_{1\_s} + \Delta D_1 \quad \text{.....(7)}$$

where V_{out_s}, V_{in_s}, I_{avg_s} and D_{1_s} are the output voltage, the input voltage, the average input current and the duty ratio at steady state, and Δv_{out}, Δv_{in}, Δi_{avg} and ΔD_1 are the small signals of the output voltage, the input voltage, the average input current and the duty ratio, respectively. In the current design step, the input and output voltages are considered to be at the steady state. Consequently, the small signals of the input voltage and the output voltage, i.e. the input and output voltage dynamics are considered to be negligible. By substituting (4)-(7) into (3), (8) is obtained,

$$\frac{L}{V_{out\_s}}\frac{d\left(\Delta i_{avg}\right)}{dt} = \frac{V_{in\_s} - V_{out\_s}}{V_{out\_s}} + D_{1\_s} + \Delta D_1 \quad \text{.....(8)}$$

The values of the input voltage, the output voltage and the duty-ratio at steady state are determined by letting the left-hand side of differential equation (8) and the small signal of the duty ratio ΔD_1 equal to zero,

$$D_{1\_s} = \frac{V_{out\_s} - V_{in\_s}}{V_{out\_s}} \quad \text{.....(9)}$$

Substituting (9) into (8) and applying the Laplace transform, then the duty-ratio-to-inductor-current transfer function in CCM is

given by (10),

$$G_{CCM}(s) = \frac{\Delta i_{avg}(s)}{\Delta D_1(s)} = \frac{V_{out\_s}}{sL} \quad \text{.....(10)}$$

Fig. 4 depicts the current control system in CCM designed based on (3) and (10). The integral period T_i and the proportional gain K_p of PI controller are designed based on the second-order standard form expressed by (11),

$$G_{2nd-order-delay}(s) = \frac{{\omega_c}^2}{s^2 + 2\zeta\omega_c s + {\omega_c}^2} \quad \text{.....(11)}$$

where ω_c is the cutoff angular frequency and ζ is the damping factor, which are designed in order to achieve the desired current response. The closed loop transfer function of the current control loop in Fig. 4 is derived by (12),

$$H_{CCM}(s) = \frac{i_{avg}(s)}{{i_{avg}}^*(s)} = \frac{\frac{K_p V_{out\_s}}{LT_i}(1 + sT_i)}{s^2 + \frac{K_p V_{out\_s}}{L}s + \frac{K_p V_{out\_s}}{LT_i}} \quad (12)$$

In order to make the design of PI parameters simple, a low pass filter whose role is to filter the command current ${i_{avg}}^*$ is necessary for matching (11) and (12). However, a low pass filter is not essentially required. Matching (11) and (12), the PI parameters are obtained by (13) and (14),

$$K_p = \frac{2\zeta\omega_c L}{V_{out\_s}} \quad \text{.....(13)}$$

$$T_i = \frac{2\zeta}{\omega_c} \quad \text{.....(14)}$$

The digital PI controller has the same coefficients as the analogous controller. To sum up, the design of the controller is performed in the frequency domain, whereas for the digital implementation, the obtained parameters are linked to the parameters of a digital PI controller [15].

B. Proposed Nonlinearity Compensation for Discontinuous Current Mode

In order to design the nonlinearity compensation part for DCM, the circuit model in DCM is required. First, the average current i_{avg} and the current peak i_{peak}, which are shown in Fig. 3 can be expressed as,

$$i_{avg} = \frac{i_{peak}}{2}(D_1 + D_2) \quad \text{.....(15)}$$

$$i_{peak} = \frac{v_{in}}{L} D_1 T_{sw} \quad \text{.....(16)}$$

Substituting (16) into (15) and solving the equation for the duty ratio D_2, then the duty ratio D_2 is expressed by (17),

$$D_2 = \frac{2Li_{avg}}{D_1 T_{sw} v_{in}} - D_1 \quad \text{.....(17)}$$

Substituting (17) into (1) in order to remove the duty ratio D_2 and representing (1) as a function of only the duty ratio D_1, (18) is obtained [10].

$$L\frac{di_{avg}}{dt} = v_{in} - v_{out} + D_1 v_{out} + (v_{out} - v_{in})\left(1 - \frac{2Li_{avg}}{v_{in} D_1 T_{sw}}\right) \quad (18)$$

Then, the circuit model in DCM is established based on (18).

Fig. 5 illustrates the circuit model of the boost converter in the DCM operation which is based on (18). In CCM, the dash line part does not exist, because the average current i_{avg} equals to the half current peak $i_{peak}/2$. On the other words, this makes the

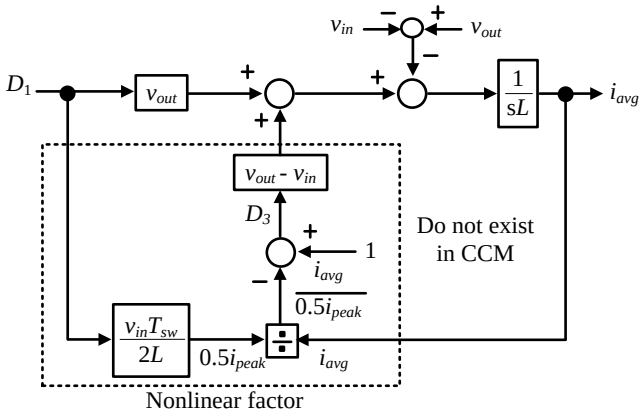

Fig. 5. Circuit model of boost converter operated in DCM. The zero-current interval D_3T_{sw} introduces the nonlinearity into the DCM transfer function, which worsens the current control performance.

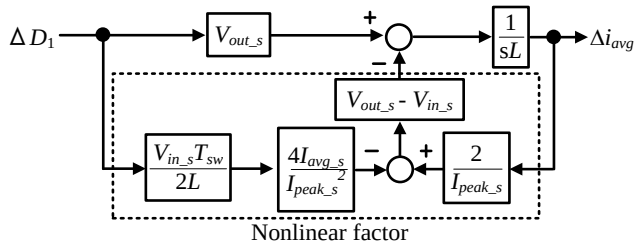

Fig. 6. Linearized circuit model. Controlling DCM by PI controller of CCM is achieved by compensating the DCM nonlinearity at the PI output.

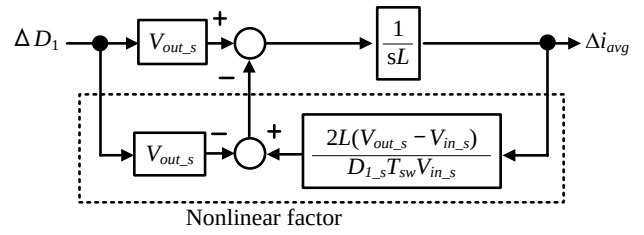

Fig. 7. Simplified and linearized circuit model. The duty ratio at steady state in the circuit model is approximated as the duty ratio at previous sampling period in order to eliminate the DCM nonlinearity.

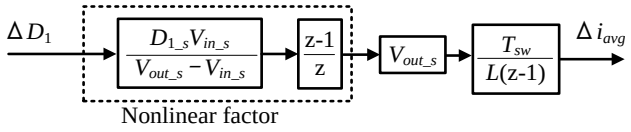

Fig. 8. Discretized circuit model. Utilizing the duty ratio at previous sampling period in order to eliminate the DCM nonlinearity makes the current control independent from inductance.

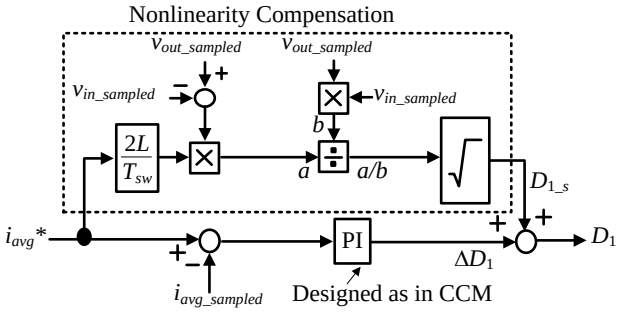

(a) Conventional DCM nonlinearity compensation in [15]-[16].

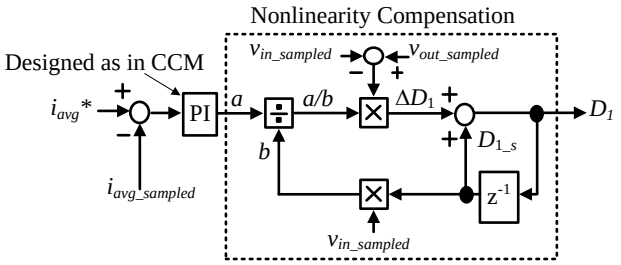

(b) Proposed DCM nonlinearity compensation.

Fig. 9. Conventional and proposed DCM nonlinearity compensation. The main difference in the proposed method is that, the DCM nonlinearity compensation is constructed by utilizing the duty ratio at the previous calculation period. This makes the control system circuit-parameter-independent and achieves the fast computation of the current control.

zero-current interval D_3T_{sw} in Fig. 3 become zero. However, in DCM, the zero-current interval introduces the nonlinearity into the DCM transfer function. This worsens the current response in DCM when same PI controller is applied for both CCM and DCM [10], [15]. Therefore, the output of the PI controller is necessary to be compensated when the circuit is operated in DCM. The design of the compensation part for the DCM nonlinearity is explained as follows. First, the circuit model in Fig. 6 is linearized at steady state.

Fig. 6 depicts the linearized circuit model. In order to simplify the coefficients in the linearized circuit model, the relationships between such coefficients at steady state are derived by substituting the differential of the inductor current di_{avg}/dt in (18) as zero and calculating the current peak,

$$I_{avg\_s} = \frac{T_{sw}}{L}\frac{D_{1\_s}^{\ 2}}{2}\frac{V_{in}V_{out}}{V_{out}-V_{in}} \quad \text{.....(19)}$$

$$I_{peak\_s} = \frac{V_{in}}{L}D_{1\_s}T_{sw} \quad \text{.....(20)}$$

where I_{avg_s}, and I_{peak_s} are the average current and the peak current at steady state, respectively. Then, (19) and (20) are substituted into Fig. 6 in order to express all coefficients as functions of D_{1_s}.

Fig. 7 depicts the simplified circuit model. In order to eliminate the dash line part in Fig. 5, in the control system, the value of D_{1_s} is approximated as the duty ratio of SW_1 at the previous calculation period $D_{1[n-1]}$. As a result, the circuit model is necessary to be analyzed in the discrete model.

Fig. 8 depicts the discretized circuit model. In order to compensate the DCM nonlinearity at the output of the PI controller designed in CCM, the dash line part in Fig. 8 is necessary to be set as 1 when the circuit is operated in DCM. Therefore, in the control system, the inverse part of the dash line part in Fig. 8 is multiplied at the output of the PI controller in order to compensate for the DCM nonlinearity.

Fig. 9 illustrates the conventional DCM nonlinearity compensation in [15]-[16], and the proposed DCM nonlinearity compensation. Note that the PI controllers in both the conventional and proposed method are designed by (13)-(14). Besides, in the power conditioning system application, the sampled input voltage which is used for the maximum power point tracking can be also used for the DCM nonlinearity compensation. The principle of two methods is the estimation of the duty ratio at steady state in order to compensate for the DCM nonlinearity. In the conventional method, the duty ratio at steady state is estimated by using current command i_{avg}^* and (19). This leads into many disadvantages: circuit-parameter-dependence, and long computation time. On the other hand, in the proposed method, the duty ratio at steady state is estimated by utilizing the duty ratio at the previous calculation period. This provides the control system circuit-parameter-independence, and short computation time. Moreover, because the dash-line part in Fig. 9(b) is always the inverse part of the nonlinear factor in Fig. 8 by utilizing the duty ratio at the previous calculation period, the DCM nonlinearity is eliminated over entire load range.

TABLE I
DUTY GENERATION OF DCM ASYNCHRONOUS SWITCHING AND DCM SYNCHRONOUS SWITCHING.

	Asynchronous Switching	Synchronous Switching
Duty-to-SW_1	D_1	D_1
Duty-to-SW_2	0	$\frac{D_1 v_{in}}{v_{out} - v_{in}}$

TABLE II
PARAMETERS OF CIRCUIT AND CONTROLLERS IN EXPERIMENTS.

Symbol	Quantity	Value
V_{in}	Input Voltage	180 V
V_{out}	Output Voltage	280 V
P	Rated Output Power	360 W
f_{sw}	Switching Frequency	20 kHz
	Frequency Analysis Simulation & Current Step Response − Load Transient Response Experiment	
Δi_{HCR}	Current Ripple at Rated Load	100% (High)
Δi_{LCR}	Current Ripple at Rated Load	10% (Low)
L_{HCR}	High Current Ripple Inductance	655 μH
L_{LCR}	Low Current Ripple Inductance	6680 μH
i_{ac}	Injected AC current (Magnitude)	0.5 A (0.25 p.u.)
f_{iac}	Injected AC current (Frequency)	0.1-5 kHz
v_{ac}	Injected AC voltage (Magnitude)	0.1 p.u.
f_{vac}	Injected AC voltage (Frequency)	0.1-100 kHz
i_{dc}	Offset of AC current command	1.25 A
f_c	Cutoff frequency (Current Con.)	2 kHz
ζ_c	Damping factor (Current Con.)	0.707
C	Output Capacitance	33 μF
f_v	Cutoff frequency (Voltage Con.)	0.2 kHz
ζ_v	Damping factor (Voltage Con.)	0.707
	Efficiency Comparison	
	Switching device	TPH3006PS (Transphorm)

C. Realization of Synchronous Switching in Discontinuous Current Mode

Fig. 10 depicts two switching patterns which occur in DCM when the switch (MOSFET) is used instead of the upper diode. This converter can improve the efficiency because the conduction loss of MOSFET is smaller than that of diode. This converter can realize three operation modes at light load depending on the turn on and off of SW_2; i) Simple CCM synchronous switching in which SW_2 is switched alternately to SW_1, ii) DCM asynchronous switching in which SW_2 is turned off at light load and iii) DCM synchronous switching in which SW_2 is turned on only during the period D_2T_{sw} as depicted in Fig. 3.

The boost inductor current of the simple CCM synchronous switching becomes continuous. Therefore, the boost inductor current ripple is constant. However, the boost inductor current increases at light load compared to that of the conventional circuit which is shown in Fig. 2. In order to improve the efficiency at light load, the DCM asynchronous switching is applied. Although the DCM asynchronous switching can reduce the boost inductor current in light load, the conduction loss of the body diode in the MOSFET is still high. In the DCM synchronous switching, in case that SW_2 is turned on exactly only in period D_2T_{sw}, the current flows through MOSFET. As a result, the conduction loss is reduced.

The main key of the DCM synchronous switching technique is to detect or estimate the moment when the current reaches zero in order to turn off SW_2. The zero-current period can be detected by comparing the detected current with a threshold value [17] or by the modified Gate Drive Unit (GDU) in [19]. However, both techniques suffers following penalties; the experimental tuning of the threshold value in the current detection or the complex GDU. In order to realize the DCM synchronous switching without any modifications of the main circuit, the duty ratio D_2 is calculated by (21) in the proposed DCM feedback control and (22) in the conventional DCM feedforward control [9], respectively,

$$D_{2\_prop\_fb} = D_1 \frac{v_{in}}{v_{out} - v_{in}} \quad \text{..... (21)}$$

$$D_{2\_conv\_ff} = \sqrt{\frac{2Li^*_{avg}(v_{out} - v_{in})}{T_{sw} v_{in}^2}} \frac{v_{in}}{v_{out} - v_{in}} \quad \text{.(22)}$$

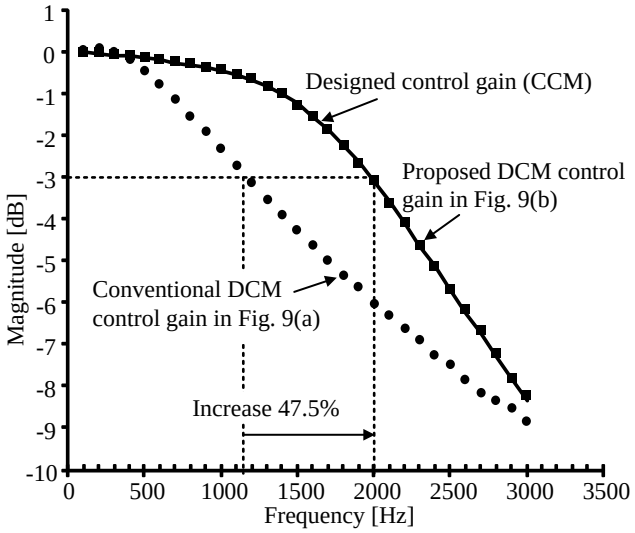

Fig. 11. Frequency characteristics of conventional and proposed DCM current feedback control. The agreement between the proposed DCM control gain and the designed gain confirms the complete elimination of the DCM nonlinearity, whereas the conventional DCM control gain results in high error of 47.5%.

Table I illustrates the duty generation of the DCM asynchronous switching and the DCM synchronous switching. Because of the mismatch between the nominal values and the actual values, the duty ratio calculated from the feed forward control method in (22) makes SW_2 turn off too early or too late when the inductor current reaches zero. This leads to the increase of the switching losses and the conduction losses. On the other hand, the duty ratio D_1 calculated from the feedback control method in (21) represents precisely for the value of the inductor current. This enables SW_2 to be turned off exactly at the moment when the inductor current

reaches zero, which results in Zero Current Switching (ZCS).

IV. Experimental Results

Table II shows the parameters of circuit and controllers in experiments. While the proposed DCM compensation is applicable for the boost converter at any power rate and any switching frequency, a boost converter is designed for a specific switching frequency at 20 kHz due to the computation time limitation of the low cost controller. Besides, the sampling method for the instantaneous average current in DCM which has been described thoroughly in [15]-[16] is also applied simply in the proposed DCM current control.

A. Frequency Analysis, Current Step Response and Load Transient Response

Fig. 11 illustrates the frequency characteristics of the conventional and proposed DCM current feedback control as shown in Fig. 9. From Table II, it is noted that the magnitude of the injected AC current command is 0.25 p.u., which can be considered as a large signal. This makes the elimination of nonlinearity in DCM by the proposed control be confirmed not only in the small-signal model but also in the large-signal model. Besides, the designed gain in Fig. 11 is calculated from the discretized second-order standard form which is derived from (11). Note that the frequency analysis is conducted in the simulation in order to confirm the cutoff frequency between the conventional and proposed DCM current feedback control. As shown in Fig.11, the frequency characteristic of the proposed DCM control agrees exactly with the designed values (CCM), whereas the cutoff frequency of the conventional DCM control results in high error of 47.5%. Furthermore, the relationship between the cutoff frequency of the outer voltage control loop and the output capacitance is expressed as (23) [1],

$$C = \frac{\Delta I_{load}}{2\pi V_{overshoot} f_v} \quad \text{.....(23)}$$

where C is the output capacitance, ΔI_{load} is the load current variation, $V_{overshoot}$ is the overshoot voltage during the load transient variation and f_v is the cutoff frequency of the outer voltage control loop. It can be understood from (23) that, under the same condition of the load current variation ΔI_{load} and the overshoot voltage $V_{overshoot}$, the output capacitance can be minimized by a wide voltage control bandwidth. Besides, the cutoff frequency f_v of the outer voltage control loop depends linearly on the cutoff frequency of the inner current control loop [18]. Hence, the bandwidth of the outer voltage control loop can be improved by 47.5% with the proposed DCM current control comparing to the voltage control bandwidth of the conventional DCM current control. As a result, the output capacitance C can be minimized by 47.5% with the proposed DCM current control.

In this paper, the implementation of the proposed DCM nonlinearity is carried out by the simplified model as shown in Fig. 6, in which the complete model in Fig. 5 is linearized and the small signal of the output voltage, i.e. the output voltage dynamic is neglected. This simplification can be considered to be reasonable in PFC applications where the output capacitor is designed based on the line frequency. However, for DC-DC conversion applications, the output voltage dynamic has to be considered in the DCM nonlinearity compensation. Therefore, AC voltages at different frequency are injected into the output voltage in order to investigate the simplification of the output voltage dynamic in the proposed DCM nonlinearity compensation.

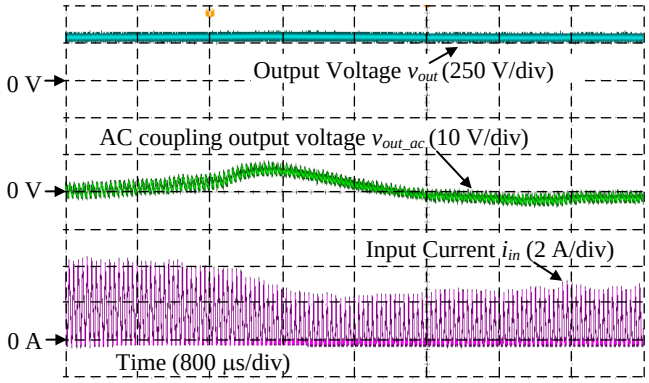

(a) Load step change: 1.0 p.u. to 0.4 p.u.

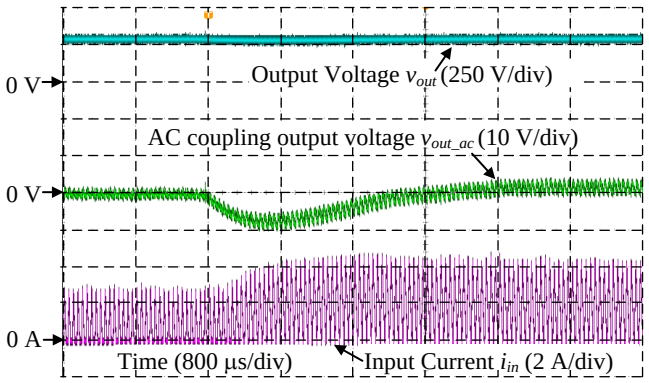

(b) Load step change: 0.4 p.u. to 1.0 p.u.

Fig. 14. Load transient response by output voltage control with 0.2-kHz cutoff frequency. The overshoot voltage and the settling time are 9 V and 1660 µs, the errors of which compared to the designed values are 4.3% and 1.6%, respectively [18].

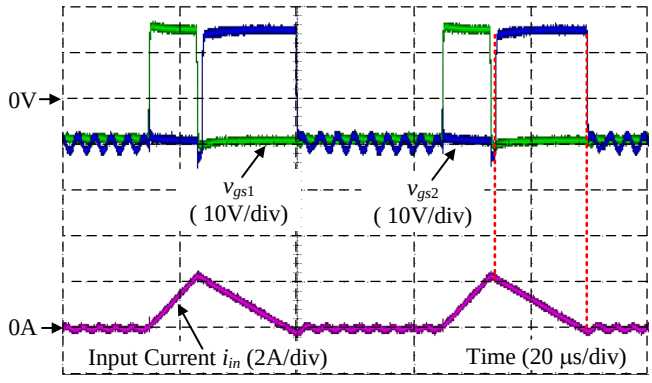

(a) Switching signal at light load (0.3 p.u.).

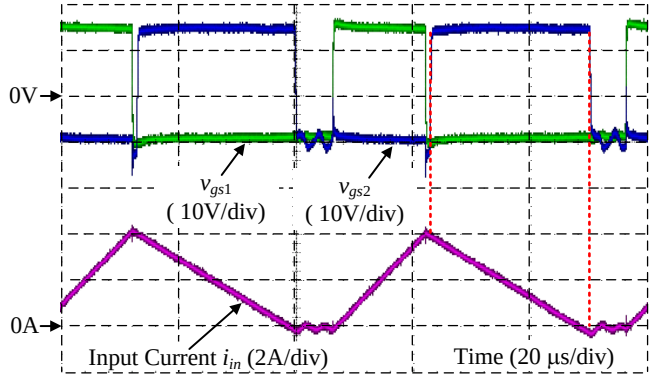

(b) Switching signal at heavy load (0.9 p.u.).

Fig. 15. DCM synchronous switching. SW_2 is turned off exactly when the current reaches zero, which achieves ZCS.

Fig. 12 depicts the frequency characteristics of the closed-loop transfer function between average inductor current and its reference, when the proposed DCM nonlinearity compensation is implemented, using the simplified model and the complete model that includes also the output voltage dynamic. It is understood from Fig. 12 that a resonance occurs due to the second-order nature of the transfer function between the duty-ratio and the inductor current [10]. Apart from that, the maximum gain difference between the simplified model and the complete model is below 0.5 dB. Consequently, in the proposed DCM nonlinearity compensation, the output capacitor is required to be designed so that the frequency of the output voltage dynamic is much higher than the cutoff frequency of the current control loop.

Fig. 13 illustrates the current step response obtained in experiment by the input current control with 2-kHz cutoff frequency at the switching frequency of 20 kHz. It is concluded that the DCM current response almost agrees with the conventional CCM current response. This confirms the validity of the proposed DCM nonlinearity compensation by experiment. Furthermore, the DCM nonlinearity compensation part is designed independently from the PI controller. Therefore, in order to further improve the performance of the DCM current control, the PID controller or the IP controller, which have been researched thoroughly for CCM operation, can be applied simply. Note that when the boost converter operates in CRM, the proposed DCM control can still be applied. However, the DCM nonlinearity compensation is required to be deactivated when the boost converter operates in CCM.

Fig. 14 shows the load transient response obtained in experiment by the output voltage control with 0.2-kHz cutoff frequency. The test is conducted with the load current step from 0.4 p.u. to 1 p.u. and vice versa. The overshoot voltage and the settling time are 9 V and 1660 µs, the errors of which compared to the designed values are 4.3% and 1.6%, respectively. The stability of the voltage control in the proposed DCM control is similar to that in the conventional CCM control because the nonlinearity in the DCM current control is eliminated completely. Consequently, this implies that the bandwidth voltage control in DCM can be increased at least as same as CCM in order to minimize the output capacitance because the DCM operation can also eliminate the right-half plan zero in CCM [20].

B. Discontinuous-Current-Mode Synchronous Switching Operation Waveforms, and Comparison of Efficiency and Computation Time

Fig. 15 illustrates the synchronous switching waveforms in DCM. It is concluded that SW_2 is turned off exactly when the current reaches zero, which achieves ZCS. Furthermore, before SW_2 is turned on, during the dead time, the current flows through the diode.

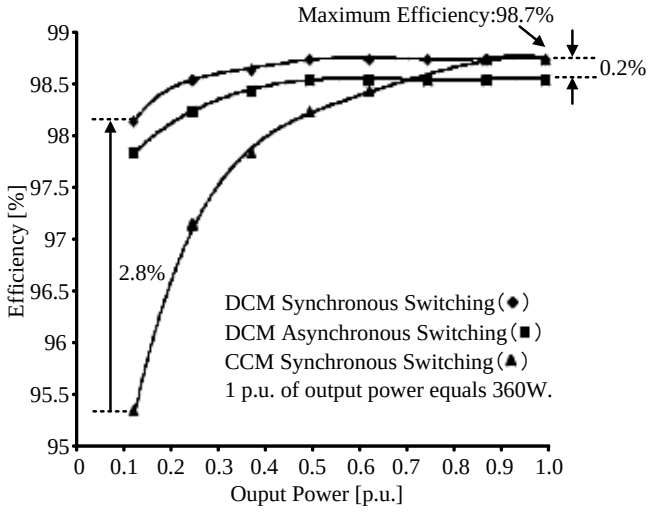

Fig. 16. Efficiency comparison among CCM synchronous switching, DCM synchronous switching and DCM asynchronous switching. The efficiency is maintained at high value above 98% over wide load range.

TABLE III
COMPUTATION TIME IN CLOCK CYCLES FOR CURRENT CONTROL LOOP.

Computation Time	CCM Current Control	Conventional DCM Current Control	Proposed DCM Current Control
PI controller	9	9	9
Duty-ratio feedforward	16	0	0
Nonlinearity compensation	0	39	22
Total	25 (1 p.u.)	48 (1.9 p.u.)	31 (1.2 p.u.)

Therefore, SW_2 turns on at the forward voltage of the diode, which is considered as ZVS. As a result, the synchronous switching in DCM causes almost no switching loss in SW_2. Furthermore, this proposed DCM synchronous switching can be realized without modifying the main circuit, which implies that the conversion efficiency can be increased simply.

Fig. 16 illustrates the efficiency comparison among the CCM synchronous switching, the DCM synchronous switching, and the DCM asynchronous switching with the same inductor L_{HCR}. The maximum efficiency of the DCM synchronous switching and the CCM synchronous switching are same as 98.7% because the circuit is designed in order to operate in CRM at full load. As the load becomes lighter, the efficiency of the CCM synchronous switching decreases as explained in Fig. 1, whereas the efficiency of the DCM synchronous switching is still maintained at high values over than 98%. In particular, at load of 0.125 p.u., the efficiency is improved by 2.8% when the DCM synchronous switching is applied. This efficiency improvement especially benefits the application with a frequent variation between light load operation and full load operation. On the other hand, compared to the DCM asynchronous switching, the efficiency of the DCM synchronous switching is higher by 0.2% at all load range. This efficiency improvement is because the conduction loss of MOSFET is lower than that of a diode in the given switching device.

Table III shows the approximate computation time for all the arithmetic operations in the current control loop. Both division and square root digital calculations are time-consuming computation involving multiple clock cycles. In particular, when a STM32 Cortex-M4 microcontroller is applied to process 32-bit floating-point single-precision data, 14 clock cycles are required for a division or square root calculation, whereas 1 clock cycle is required for an addition or subtraction and 3 clock cycles are required for a multiplication [21]. In the conventional DCM current control, a division followed by a square root calculation is required to compute the DCM duty ratio as shown in Fig. 9(a). On the other hand, only one division is required in both the CCM current control as in Fig. 4 and the proposed DCM current control as in Fig. 9(b). Consequently, the computation time of the proposed DCM current control is longer only 6 clock cycles than the CCM current control, whereas the conventional DCM current control requires 35% longer computation time than the proposed DCM current control. Therefore, the proposed DCM current control helps in reducing the cost of the controller.

V. CONCLUSION

The approach to deal with the nonlinearity of DCM in this paper was to utilize the duty ratio at the previous calculation period. This provided both the complete elimination of the DCM nonlinearity and the short computation time. Furthermore, the simple DCM synchronous switching without any modifications of the main circuit was realized to achieve high efficiency above 98% over wide load range, which helped in reducing the power consumption under light load conditions. In comparison with the CCM current control, the proposed DCM current control achieves the same current control bandwidth and improves the light load efficiency by 2.8% at most. Furthermore, the proposed DCM current control not only reduces the computation time by 35% but also increases the current control bandwidth by 47.5% compared to the conventional DCM current control. Consequently, the proposed DCM current control contributes into both the downsizing of the boost converter by the wide bandwidth current and voltage control, and the high efficiency over wide load range as well as short computation time.

ACKNOWLEDGMENT

The authors would like to thank Dr. Hiroki Takahashi and Dr. Keisuke Kusaka, Power Electronics Laboratory, Nagaoka University of Technology, Nagaoka, Japan, for constructive advice and collaboration.

REFERENCES

[1] K. Yao, Y. Ren, and F. C. Lee, "Critical Bandwidth for the Load Transient Response of Voltage Regulator Modules," *IEEE Trans. Power Electron.*, vol. 19, no. 6, pp. 1454-1461, Nov. 2004.

[2] B. A. Ferrari, N. R. N. Ama, K. C. M. Carvalho, F. O. Martinz, and L. M. Junior, “Robust Control Design for Voltage Tracking Loop of Dynamic Voltage Restorers,” *IEEJ J. Ind. Appl.*, vol. 4, no. 5, pp. 634-642, Sep. 2015.
[3] R. C. N. Pilawa-Podgurski, A. D. Sagneri, J. M. Rivas, D. I. Anderson, and D. J. Perreault, “Very-High-Frequency Resonant Boost Converters,” *IEEE Trans. Power Electron.*, vol. 24, no. 6, pp. 1654-1665, Jun. 2009.
[4] H. Kosai, S. McNeal, B. Jordan, J. Scofield, B. Ray, and Z. Turgut, “Coupled Inductor Characterization for a High Performance Interleaved Boost Converter,” *IEEE Trans. Magnetics*, vol. 45, no. 10, pp. 4812-4815, Oct. 2009.
[5] A . B. Ponniran, K. Matsuura, K. Orikawa, and J. Itoh, “Size reduction of DC-DC converter using flying capacitor topology with small capacitance,” *IEEJ J. Ind. Appl.*, Vol. 3, No. 6, pp. 20-30, Nov. 2014.
[6] J. Imaoka, M. Yamamoto, and T. Kawashima, “High-Power-Density Three-phase Interleaved Boost Converter with a Novel Coupled Inductor,” *IEEJ J. Ind. Appl.*, vol. 4, no. 1, pp. 20-30, Jan. 2015.
[7] T. Masuzawa, E. Hoene, S. Hoffmann, and K. Lang, “Modeling Method of Stray Magnetic Couplings in an EMC Filter for Power Electronic Devices”, *IEEJ J. Ind. Appl.*, vol. 4, no. 6, pp. 738-744, Nov. 2015.
[8] J. Zhang, J. Sh. Lai, R. Y. Kim, and W. Yu, “High-Power Density Design of a Soft-Switching High-Power Bidirectional dc–dc Converter”, *IEEE Trans. Power Electron.*, vol. 22, no. 4, pp. 1145-1153, Jul. 2007.
[9] L. Ni, D. J. Patterson, and J. L. Hudgins, “High Power Current Sensorless Bidirectional 16-Phase Interleaved DC-DC Converter for Hybrid Vehicle Application,” *IEEE Trans. Power Electron.*, vol. 27, no. 3, pp. 1141-1151, Mar. 2012.
[10] Jian Sun, Daniel M. Mitchell, Matthew F. Greuel, Philip T. Krein, and Richard M. Bass: “Averaged Modeling of PWM Converters Operating in Discontinuous Conduction Mode,” *IEEE Trans. Power Electron.*, vol.16, no. 4, pp.482-492, Jul. 2001.
[11] A. Saysanasongkham, M. Arai, S. Fukumoto, S. Takeuchi, and K. Wada, “A Highly Reliable Digital Current Control using an Adaptive Sampling Method,” *IEEJ J. Ind. Appl.*, vol. 3, no. 4, pp. 296-303, Jul. 2014.
[12] T. S Hwang, and S. Y. Park, “Seamless Boost Converter Control Under the Critical Boundary Condition for a Fuel Cell Power Conditioning System,” *IEEE Trans. Power Electron.*, vol. 27, no. 8, pp. 3616-3626, Aug. 2012.
[13] J. W. Shin, and B. H. Cho, “Digitally Implemented Average Current-Mode Control in Discontinuous Conduction Mode PFC Rectifier,” *IEEE Trans. Power Electron.*, vol. 27, no. 7, pp. 3363-3373, Jul. 2012.
[14] K. D. Gusseme, D. M. V. de Sype, A. P. V. den Bossche, J. A. Melkebeek, “Sample correction for digitally controlled boost PFC converters operating in both CCM and DCM,” in *Proc. 18th Annu. IEEE Appl. Power Electron. Conf. Expo.*, Feb. 2003, pp. 389–395.
[15] K. D. Gusseme, D. M. V. de Sype, A. P. V. den Bossche, and J. A. Melkebeek, “Digitally Controlled Boost Power-Factor-Correction Converters Operating in Both Continuous and Discontinuous Conduction Mode,” *IEEE Trans. Power Electron.*, vol. 52, no. 1, pp. 88-97, Feb. 2005.
[16] Sh. F. Lim, and A. M. Khambadkone, “A Simple Digital DCM Control Scheme for Boost PFC Operating in Both CCM and DCM,” *IEEE Trans. Power Electron.*, vol. 47, no. 4, pp. 1802-1812, Aug. 2011.
[17] C. W. Clark, F. Musavi, and W. Eberle, “Digital DCM Detection and Mixed Conduction Mode Control for Boost PFC Converters,” *IEEE Trans. Power Electron.*, vol. 29, no. 1, pp. 347-355, Jan. 2014.
[18] S. W. Kang, H. J. Kim, and B. H. Cho, “A Dual-Loop Voltage Control for Optocoupler Feedback in Capacitive Output Filter Converter,” in *Proc. IEEE Energy Convers. Congr. Expo.*, Oct. 2015, pp. 20-24.
[19] J. Wan, F. Zheng, Y. Zhang, P. Wang, X. Yang, and D. Bai, “A new control method for boost converter in discontinuous conduction mode with synchronous rectification and zero voltage switching,” in *Proc. IEEE Energy Convers. Congr. Expo. Asia*, Aug. 2013, pp. 650-654.
[20] S. Kapat, A. Patra, and S. Banerjee, “A Current Controlled Tri-State Boost Converter with Improved Performance through RHP Zero Elimination,” *IEEE Trans. Power Electron.*, vol. 24, no. 3, pp. 776 - 786, Mar. 2009.
[21] Floating point unit demonstration on STM32 microcontrollers, Application note, May 2016, STMicroelectronics.